Indium Doping in Barium Cerate: the Relation between Local Symmetry and the Formation and Mobility of Protonic Defects

Francesco Giannici,*[,†] Alessandro Longo,[‡] Antonella Balerna,[§] Klaus-Dieter Kreuer,[||] and Antonino Martorana[†]

Dipartimento di Chimica Inorganica e Analitica "Stanislao Cannizzaro", Università di Palermo, Viale delle Scienze, I-90128 Palermo, Italy, Istituto per lo Studio dei Materiali Nanostrutturati, Consiglio Nazionale delle Ricerche, Via Ugo La Malfa, 153, I-90146 Palermo, Italy, Laboratori Nazionali di Frascati, Istituto Nazionale di Fisica Nucleare, Via Enrico Fermi 44, I-00044, Frascati, Italy, and Max-Planck-Institut für Festkörperforschung, Heisenbergstrasse 1, D-70569 Stuttgart, Germany

Received July 18, 2007. Revised Manuscript Received September 10, 2007

The solid solution series $Ba(In,Ce)O_{3-\delta}$ has been investigated with respect to structure, formation, and mobility of protonic defects. Compared to the limited solubility of Y_2O_3 in $BaCeO_3$ and $BaZrO_3$, the complete solubility of In_2O_3 is suggested to reflect a relation between absolute hardness of the dopant and the ease of insertion into the hosting lattices. Extended X-ray absorption fine structure (EXAFS) was used to probe the local environment of In^{3+} in barium cerate: in the surroundings of the dopant, the orthorhombic structure is strongly modified, resulting in an increase of local symmetry. The InO_6 octahedra are very regular, and there is no indication for any defect clustering. This is suggested to be the main reason for the low entropy of formation of protonic defects by water dissolution. The mobility of such defects is slightly lower than in Y-doped $BaCeO_3$, but at high dopant levels the high local symmetry allows for formation of very high concentrations of protonic defects. This leads to high proton conductivities, which render In^{3+} an attractive dopant for $BaCeO_3$-based proton conductors.

1. Introduction

If a II−IV perovskite like $BaCeO_3$ is doped with a trivalent cation on the B site, inducing oxygen vacancies to preserve charge balance, protonic defects can be inserted into the lattice according to

$$H_2O + O_O^x + V_O^{\bullet\bullet} = 2OH_O^{\bullet} \quad (1)$$

The properties of doped proton-conducting perovskites have been extensively reviewed recently.[1,2] While reported conductivities are not yet sufficiently high for fuel cell applications,[3] such materials may well be used as separators in H_2 purifiers, sensors, and other electrochemical devices.[4]

In the ABO_3 perovskite structure the smaller B cation, usually tetravalent, resides in the center of corner-sharing BO_6 octahedra. The larger bivalent A cation is located in the cavities between eight octahedra with a 12-fold oxygen coordination. For an ideal perovskite, like $CaTiO_3$, the Goldschmidt tolerance factor, defined as

$$\tau = \frac{R_A + R_O}{\sqrt{2}(R_B + R_O)} \quad (2)$$

is close to unity. When its value deviates from unity, the misfit between R_A and R_B must be accommodated with some kind of distortion. In the case of barium cerate, Ce^{4+} is slightly too big compared to Ba^{2+}, and for $\tau = 0.94$ the resulting structure is orthorhombic (*Pmcn* space group). In barium zirconate, on the contrary, Zr^{4+} fits almost perfectly on the B site: thus, the tolerance factor is about 1 and the symmetry is cubic.

In general, the highest protonic conductivity among barium cerates and zirconates is observed in the case of Y^{3+} doping, followed by Gd^{3+} and other lanthanides. Current development of proton-conducting perovskites for electrochemical applications is presently stuck with two issues: (1) materials with high conductivity (barium cerates) have awkward mechanical properties and chemical resistance and (2) materials with good mechanical properties and chemical resistance (barium zirconate) show very high grain boundary impedance and sintering problems. To achieve both high stability and conductivity, barium cerates/zirconates mixtures have been investigated: recent synthetic approaches have relied on core−shell structures[5] or on single phases with ZnO as a sintering aid.[6−7] However, these attempts have not yet

* To whom correspondence should be addressed. E-mail: giannici@pa.ismn.cnr.it.
† Università di Palermo.
‡ Istituto per lo Studio dei Materiali Nanostrutturati.
§ Istituto Nazionale di Fisica Nucleare.
|| Max-Planck-Institut für Festkörperforschung.

(1) Kreuer, K.-D. *Annu. Rev. Mater. Res.* **2003**, *33*, 333.
(2) Kreuer, K.-D.; Paddison, S. J.; Spohr, E.; Schuster, M. *Chem. Rev.* **2004**, *104*, 46.
(3) Steele, B. C. H.; Heinzel, A. *Nature* **2001**, *414*, 345.
(4) Iwahara, H.; Asakura, Y.; Katahira, K.; Tanaka, M. *Solid State Ionics* **2004**, *168*, 299.
(5) Savaniu, C. D.; Canales-Vazquez, J.; Irvine, J. T. S. *J. Mater. Chem.* **2005**, *15*, 598.
(6) Babilo, P.; Haile, S. M. *J. Am. Ceram. Soc.* **2005**, *88*, 2362.
(7) Tao, S.; Irvine, J. T. S. *Adv. Mater.* **2006**, *18*, 1581.

10.1021/cm701902p CCC: $37.00
Published on Web 10/16/2007

sufficiently reduced the grain boundary impedance as the total conductivity lies about 2 orders of magnitude below the Y:$BaZrO_3$ bulk conductivity.

Despite the various synthetic efforts to find the best combination of cations for optimum stability and performance, many fundamental aspects are still unclear as evidenced in several recent papers dealing with (1) dopant−defect interactions,[8−11] (2) relations between oxide basicity and conductivity,[12,13] and (3) anomalous behavior in water incorporation.[14] When the local environment around the doped B sites is very different from undoped ones it is not possible to get a correct picture of the lattice using only diffraction techniques. X-ray absorption spectroscopy (XAS) is the only technique able to selectively probe a single element in a complex matrix and then, by modeling the extended X-ray absorption fine structure (EXAFS), determine the local environment of the selected element with high accuracy. Although less exploited than diffraction, XAS is a very important technique in solid-state studies, and its importance for structural analysis of the local environment of dopants is outstanding. It is somewhat surprising that it was only few years ago that it started to be used to study proton-conducting perovskites.[15,16]

The traditional criterion of ionic radius matching is a successful strategy for doping anionic conductors with aliovalent cations,[17,18] but much evidence has demonstrated that this criterion is not the only one effective for protonic conductors. In particular, chemical matching has been suggested to be an additional criterion for a suitable dopant.[13] It is interesting to note that Y^{3+}, usually regarded as "the ideal dopant" for Ce^{4+}, only partially fulfills these criteria. Using EXAFS we recently elucidated the effects of Y^{3+} insertion into the barium cerate host lattice:[19,20] (i) despite the very small ionic radius mismatch of 0.03 Å,[21] YO_6 octahedra are axially distorted; (ii) protonic defects preferentially interact with doped B sites. Moreover, the dopant solubility limit is less than 20% of the available B sites, and therefore, the possibility of introducing protonic defects into the matrix is also limited. In conclusion, it was observed that Y^{3+} is far from being the ideal dopant, introducing a different positive charge into the host lattice but leaving the matrix substantially unperturbed. On the basis of this evidence, we desired to study other dopants of the B site of $BaCeO_3$ with the aim of investigating the relative importance of structural and chemical factors. This paper is devoted to the study of the behavior of In^{3+} as B-site dopant.

In^{3+} has very rarely been taken into account in the literature as a dopant for proton-conducting perovskites, although at present the only commercialized device based on this class of materials uses as electrolyte In:$CaZrO_3$.[22,23] There are almost no investigations on In:$BaCeO_3$ (from now on BCI; the acronym is followed by a number indicating the dopant percentage), and only recently In:$BaZrO_3$ (from now on BZI) has been characterized by a thorough crystallographic and functional study.[24] On the other hand, the related compound $Ba_2In_2O_5$, with brownmillerite structure, has been the subject of a great number of papers for its possible applications as both anion and proton conductor.[25−30] In this paper the structural and functional characterization of In-doped barium cerate is reported together with particular attention to indium solubility and proton−dopant interactions. The study was carried out using different structural techniques (XRD, EXAFS), thermogravimetric analysis, and impedance spectroscopy. Useful information to understand some experimental results is given by the comparison with In-doped barium zirconates and other oxides.

2. Experimental Section

2.1. Materials and Synthesis. Barium carbonate (99%, Merck), cerium oxide (99.9%, Alfa Aesar), and indium oxide (99.9%, Alfa Aesar) were used as starting compounds. The powders were mixed in ethanol, calcined at 1100 °C for 2 h, ball milled for 1 h, calcined at 1300 °C overnight, and planetary milled for 2 h. A portion of the powders was dried in pure N_2 at 600 °C for 6 h to completely remove protons. For conductivity measurements, the powders were isostatically pressed at 800 MPa and sintered at 1400 °C for 12 h (heating rate 100 K/h, cooling rate 50 K/h) in air. The relatively low sintering temperature was chosen to avoid any volatile compound loss. The pellets were then polished, painted with Pt paste, and fired at 1000 °C for 1 h.

2.2. Thermogravimetry and Impedance Spectroscopy. Thermogravimetric data were recorded with a thermostated Sartorius 7014 balance with $pH_2O = 23$ hPa using N_2 as a carrier gas. After cooling from 800 to 200 °C, further heating to 300 °C showed no hysteresis, so we assumed that TGA values collected on cooling represent thermodynamic equilibrium. Conductivity data were recorded using a Hewlett-Packard LCR Meter 4284A in the same gas conditions as TGA. The impedance spectra were collected from 50 to 880 °C and modeled with ZView.

(8) Islam, M. S.; Davies, R. A.; Gale, J. D. *Chem. Mater.* **2001**, *13*, 2049.
(9) Islam, M. S.; Slater, P. R.; Tolchard, J. R.; Dinges, T. *Dalton Trans.* **2004**, 3061.
(10) Hempelmann, R.; Karmonik, C.; Matzke, T.; Cappadonia, M.; Stimming, U.; Springer, T.; Adams, M. A. *Solid State Ionics* **1995**, *77*, 152.
(11) Kreuer, K.-D.; Münch, W.; Ise, M.; Fuchs, A.; Traub, U.; Maier, J. *Ber. Bunsen-Ges. Phys. Chem.* **1997**, *101*, 1344.
(12) Kreuer, K.-D. *Solid State Ionics* **1999**, *125*, 285.
(13) Kreuer, K.-D.; Adams, S.; Münch, W.; Fuchs, A.; Klock, U.; Maier, J. *Solid State Ionics* **2001**, *145*, 295.
(14) Kruth, A.; Davies, R. A.; Islam, M. S.; Irvine, J. T. S. *Chem. Mater.* **2007**, *19*, 1239.
(15) Islam, M. S.; Davies, R. A.; Fisher, C. A. J.; Chadwick, A. V. *Solid State Ionics* **2001**, *145*, 333.
(16) Wu, J.; Webb, S. M.; Brennan, S.; Haile, S. M. *J. Appl. Phys.* **2005**, *97*, 054101-1.
(17) Inaba, H.; Tagawa, H. *Solid State Ionics* **1996**, *83*, 1.
(18) Kharton, V. V.; Marques, F. M. B.; Atkinson, A. *Solid State Ionics* **2004**, *174*, 135.
(19) Longo, A.; Giannici, F.; Balerna, A.; Ingrao, C.; Deganello, F.; Martorana, A. *Chem. Mater.* **2006**, *18*, 5782.
(20) Giannici, F.; Longo, A.; Deganello, F.; Balerna, A.; Arico, A. S.; Martorana, A. *Solid State Ionics* **2007**, *178*, 587.
(21) Shannon, R. D. *Acta Cryst., Sect. A* **1976**, *32*, 751.
(22) Yajima, T.; Koide, K.; Takai, H.; Fukatsu, N.; Iwahara, H. *Solid State Ionics* **1995**, *79*, 333.
(23) Gansemer, T. M.; Hart, J. N. *U.S. Patent 7086274.*
(24) Ahmed, I.; Eriksson, S.-G.; Ahlberg, E.; Knee, C. S.; Berastegui, P.; Johansson, L.-G.; Rundlöf, H.; Karlsson, M.; Matic, A.; Börkesson, L.; Engberg, D. *Solid State Ionics* **2006**, *177*, 1395.
(25) Zhang, G. B.; Smyth, D. M. *Solid State Ionics* **1995**, *82*, 153.
(26) Zhang, G. B.; Smyth, D. M. *Solid State Ionics* **1995**, *82*, 161.
(27) Schober, T.; Friedrich, J. *Solid State Ionics* **1998**, *113−115*, 369.
(28) Stølen, S.; Mohn, C. E.; Ravindran, P.; Allan, N. L. *J. Phys. Chem. B.* **2005**, *109*, 12362.
(29) Stølen, S.; Bakken, E.; Mohn, C. E.; Matter, S. *Phys. Chem. Chem. Phys.* **2006**, *8*, 429.
(30) Fisher, C. A. J.; Islam, M. S. *Solid State Ionics* **1999**, *118*, 355.

2.3. X-ray Diffraction. The X-ray diffraction patterns were recorded with a PW1050 diffractometer (Philips) equipped with a graphite monochromator using Cu Kα radiation in Bragg−Brentano geometry from 10° to 90° 2θ. For the in situ measurements, the sample was placed on a thermostated Pt stage in a gastight chamber (Anton Paar): in this case, the XRD patterns were collected on cooling in wet N_2, consistent with TGA measurements. The diffraction profiles were modeled with GSAS[31] using either a cubic (*Pm*-3*m*, for high In^{3+} levels) or orthorhombic (*Pmcn*,[32] for low In^{3+} levels) unit cell. Bragg peaks were modeled using pseudo-Voigt peak shape, and the background was subtracted using Chebychev polynomials. The refined parameters were the unit cell size, two profile parameters (Lorenzian broadening), three isotropic thermal parameters (one for the A site, one for the B site, and one for anions), and seven background terms. The Gaussian broadening parameters accounting for the instrumental contribution were determined using the LaB_6 standard and fixed during the fit.

2.4. X-ray Absorption. X-ray absorption spectra at the indium K-edge (27 KeV) were collected at the GILDA BM8 beamline at the European Synchrotron Radiation Facility (ESRF) using a Si (311) double-crystal monochromator on as-prepared and dried samples from BCI2 to BCI30. Measurements were taken from −193 to 600 °C in transmission or fluorescence mode (for 2%-doped samples): in the latter case, a Ge 13-element detector was used, and the monochromator was operated in sagittal focusing mode to achieve a higher photon flux (ca. 10^{11} ph/s) on the sample. High-temperature measurements in wet atmosphere were performed using an in situ thermochemical cell.[33] Unless otherwise specified, the results refer to the lowest temperature measurement. Theoretical amplitudes and phases were calculated with FEFF8.2.[34] The In_2O_3 spectrum, used as standard, was fitted to obtain reliable S_0^2 and ΔE_0 values. All the data were weighed by k^2, extracted with a Bayesian algorithm (k range = ca. 2−16 Å^{-1}), and fitted in the R space using the program Viper.[35] For the BCI2 samples, the R range used in the fitting was 1.23−6.21 Å, while for all the other samples the R range ended at 4.52 Å: this results in 30−48 independent points for 13−17 fitting parameters, which assures highly reliable fittings.

3. Results and Discussion

The long-range order in BCI has been investigated using X-ray diffraction. A comparison of the XRD patterns of as-prepared samples with different doping levels is reported in Figure 1. The low-doped materials, up to 30% In^{3+} content, are successfully refined on the basis of an orthorhombic *Pmcn* unit cell; the samples with higher In^{3+} content can be modeled using a *Pm*-3*m* cubic cell. The space group change can be clearly noticed from inspection of Figure 1, i.e., the peak widths increase when the symmetry is lowered from cubic to orthorhombic due to splitting of the Bragg reflections. In any case, the XRD patterns did not evidence any sample inhomogeneity as all patterns were suitably refined using a single crystallographic phase. Figure 2 shows the cubic root of unit cell volumes, $V^{1/3}$, as a function of the dopant concentration. The linear decrease of $V^{1/3}$ as a function of indium content in the whole compositional range is a further evidence for the complete miscibility of $BaCeO_3$ and $Ba_2In_2O_5$.

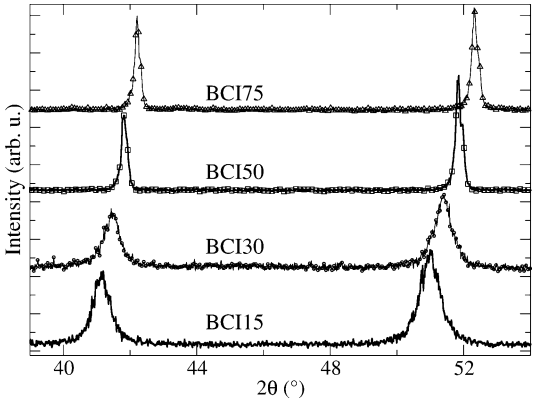

Figure 1. X-ray diffraction patterns of BCI with different doping levels in the 39−54° angular range. The BCI50 and BCI75 profiles have been multiplied by 0.5 for graphical purposes.

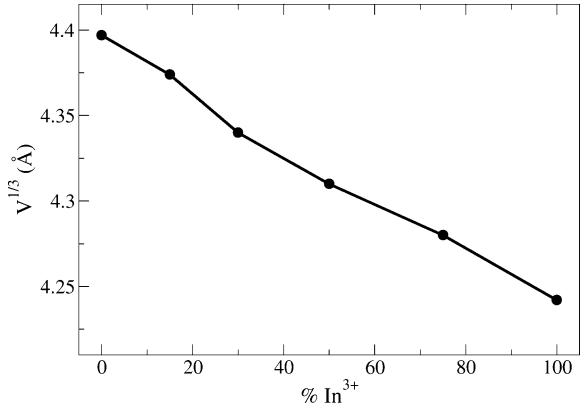

Figure 2. Pseudo-cubic lattice parameter for BCI as a function of In^{3+} content.

Recently, we demonstrated with EXAFS that yttrium solubility in barium cerate is quite low (between 15% and 20%),[20] even lower than previously determined by XRD,[36] and that a Y_2O_3 phase, undetectable by X-ray diffraction methods, is segregated at grain boundaries or in nanosized inclusions. In barium zirconate, however, Y^{3+} may be incorporated up to a solubility limit of around 15%, which seems to be strongly dependent on the preparation conditions. EXAFS results on barium cerate with doping levels as high as 30% in both In^{3+} and Gd^{3+},[37] on the contrary, do not show formation of any second phase. It is worth noting that neutron diffraction data point toward the complete miscibility of In^{3+} into barium zirconate.[24,38] In this respect, the nonlinear dependence of the lattice constant of BZI on dopant content[24] could be ascribed to defect clustering since preliminary EXAFS results on BZI did not evidence any modification of the chemical environment of In^{3+} for different compositions of BZI. Taking into account the different structure and chemical composition of BZ and BC and the quite different ionic radii of Y^{3+} and In^{3+}, it seems reasonable that the partial

(31) Larson, A.; Von Dreele, R. B. *Report LAUR* **1988**, 86.
(32) Knight, K. S. *Solid State Ionics* **2001**, *145*, 275.
(33) Longo, A.; Balerna, A.; D'Acapito, F.; D'Anca, F.; Giannici, F.; Liotta, L. F.; Pantaleo, G.; Martorana, A. *J. Synchrotron Rad.* **2005**, *12*, 499−505.
(34) Ankudinov, A. L.; Ravel, B.; Rehr, J. J.; Conradson, S. D. *Phys. Rev. B* **1998**, *58*, 7565.
(35) Klementev, K. D. *J. Phys. D: Appl. Phys.* **2001**, *34*, 209.
(36) Ma, G.; Shimura, T.; Iwahara, H. *Solid State Ionics* **1999**, *120*, 51.
(37) Longo, A.; Giannici, F.; Balerna, A.; Martorana, A. Manuscript in preparation.
(38) Berastegui, P.; Hull, S.; Garcìa-Garcìa, F. J.; Eriksson, S.-G. *J. Solid State Chem.* **2002**, *164*, 119.

Table 1. Structural Parameters of the First Four Coordination Shells around In^{3+} As Derived from EXAFS Analysis[a]

	In−O (CN = 6)		In−Ba (CN = 8)		In−M (CN = 6)		In−Ce (CN = 12)	
	R (Å)	σ^2 (10^{-3} Å^2)	R (Å)	σ^2 (10^{-3} Å^2)	R (Å)	σ^2 (10^{-3} Å^2)	R (Å)	σ^2 (10^{-3} Å^2)
BCI2	2.167	5.74	3.66	6.8	4.34	4.11	6.17	7.02
BCI2 dry	2.164	5.70	3.64	6.7	4.34	4.08	6.17	6.30
BCI15	2.154	7.27	3.59	9.2	4.35	8.24		
BCI15 dry	2.151	7.68	3.59	9.0	4.36	6.84		
BCI20	2.154	6.97	3.63	8.4	4.37	8.41		
BCI20 dry	2.148	7.32	3.60	8.3	4.37	7.02		
BCI30	2.154	6.42	3.60	8.9	4.38	8.46		
BCI30 dry	2.148	6.92	3.60	8.9	4.38	9.62		

[a] As the fourth coordination shell is visible for 2%-doped sample only, it is referred to as being composed by Ce atoms only. Uncertainty is on the last digit.

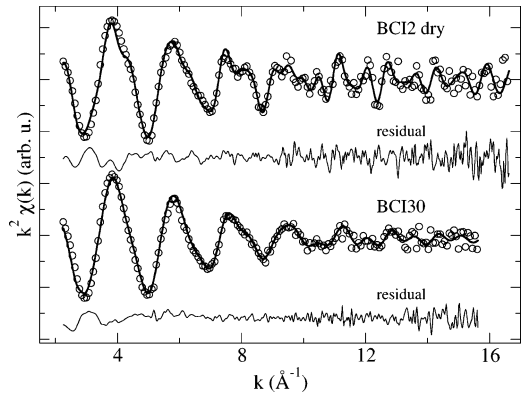

Figure 3. Experimental k^2-weighed EXAFS spectra, best fits, and residual functions for BCI2 dry and BCI30 as-prepared samples at −193 °C.

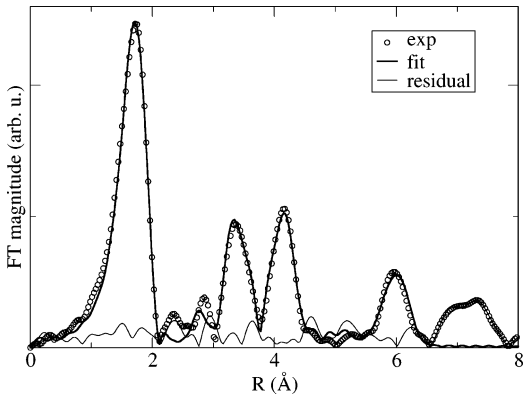

Figure 4. Fourier transform of *k*-weighed EXAFS spectrum, best fit, and residual function for dry BCI2 at −193 °C.

miscibility of yttrium and complete miscibility of indium in both perovskites could be ascribed to a different chemical behavior of these dopants.

Analysis of the EXAFS oscillations, for samples ranging from BCI2 to BCI30, yields several general results, which are summarized in Table 1. As an example of the data and fitting quality, the two extreme cases, the dry BCI2 sample and the as-prepared BCI30, are reported in Figures 3−5 together with their Fourier transforms. The first result, which holds for any sample in any hydration condition in the whole temperature range, is that InO_6 octahedra are always regular with six equivalent In−O bond lengths ranging from 2.15 to 2.17 Å (Ce−O is ca. 2.27 Å) depending on the sample. From these results, the octahedron volume contraction can be calculated, ranging from 13% to 16% for indium doping. In the case of BCY,[19] the YO_6 octahedra showed a lower expansion, of about 4%. The differences between the spectra of as-prepared and dry BCI samples are not as systematic

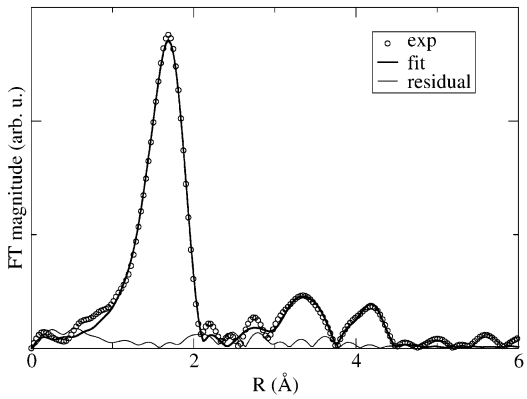

Figure 5. Fourier transform of *k*-weighed EXAFS spectrum, best fit, and residual function for as-prepared BCI30 at −193 °C.

and large as it was for the yttrium K-edge spectra of BCY. In the latter case, the Debye−Waller factors accounting for the vibrational disorder were critically affected by the proton content of the material, systematically decreasing by 30−100% when the protonic defects were removed from the lattice. For In^{3+} EXAFS data, the best-fit models yielded unsystematic variations in the disorder factors of about 5−10%, giving no hints to a direct influence of hydroxyl ions on the dopant local environment. These observations can be connected with the previously reported YO_6 octahedral distortion in yttrium-doped barium cerate[19] in arguing that vacancies/protonic defects do not preferentially interact with the In^{3+}-doped B -sites.

With respect to the second coordination shell, the EXAFS data for BCI can be satisfactorily fitted using only one In−Ba distance regardless of the doping level. In the case of BCY,[20] the Y−Ba shell was analyzed also using only one distance: in that case, however, a very high Debye−Waller factor (about 0.012 Å^2) was necessary to fit the data, while the corresponding Ce−Ba correlations were modeled using two different distances with Debye−Waller factors of about 0.006 Å^2. Since this holds for both dry and as-prepared samples, it is likely that the difference in the disorder factors is caused by static disorder, i.e., that more Y−Ba distances are actually present. The In−Ba distance is modeled with a Debye−Waller factor of about 0.009 Å^2. To confirm the presence of only one In−Ba distance, a model involving two In−Ba distances (kept 0.12 Å apart) was also used to obtain the best fit for the as-prepared BCI2 sample. The comparison of these two models, which rules out pronounced distortions, is reported in Figure 6. In conclusion, according to the EXAFS data the second coordination shell of In^{3+} is given

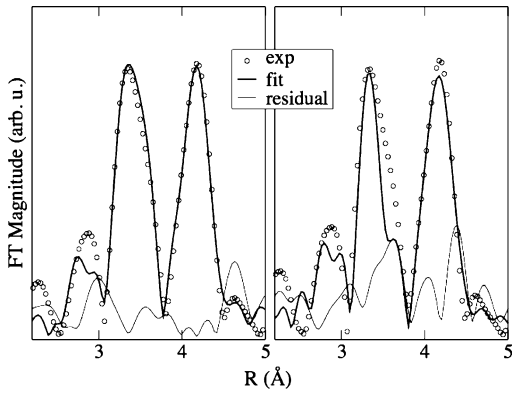

Figure 6. BCI2 best fitting using (a) one In−Ba distance and (b) two In−Ba distances kept 0.12 Å apart.

by a cube of eight Ba^{2+} ions symmetrically placed around the doped B site.

It must be noted that this behavior is present also at very low dopant content (2%), which indicates that In^{3+} minimizes the structural misfit with the host lattice by locally displacing the surrounding atoms to recreate a cubic environment around itself. This is not surprising considering the fact that the cation pair In^{3+} and Ba^{2+} is almost perfectly fulfilling the Goldschmidt criterion. In conclusion, in the BCI dopant environment, the local "distortion" is actually a local symmetry increase with respect to the globally orthorhombic host lattice. As for the oxygen octahedral shell, the $InBa_8$ cube presents a volume contraction of about 15% with respect to the corresponding $CeBa_8$ polyhedron. (In comparison in the YBa_8 polyhedron for the different BCY compounds, the expansion relative to the undoped polyhedron is lower than 5%.) The third shell, In−M (where M = Ce or In), is placed at about 4.34 Å (in BCY, the corresponding Y−M distance is 4.44 Å). The local displacement of atoms around In^{3+} is clearly due to lattice relaxation around the dopant, and for the same reason the displacement of the atoms from their crystallographic sites decreases as the distance from the dopant increases. This analysis is also confirmed by the second In−Ce coordination shell (representing the diagonal of the face of the cube with B sites in its vertices) in the 2%-doped samples: in this case, the distance is 6.18 Å, compared to 6.23 Å in the Ce^{4+} local environment. The disorder factors remarkably increase as the dopant cation concentration goes over 2%: beyond this threshold no pronounced disorder change occurs in the local structure with increasing In^{3+} content.

A high water content was already reported below 400 °C for BZI75.[24] We found a similar behavior with complete water uptake for highly doped BCI. In Figure 7 the TGA curve for BCI30 is plotted along with the evolution of the unit cell size as a function of temperature. In the low-temperature range, where the degree of hydration is temperature independent, the lattice parameter increases linearly with temperature, reflecting a simple thermal expansion. Between 350 and 550 °C the sample loses weight as a consequence of the H_2O evolution; removal of lattice $OH_O^{\bullet}$ results in a contraction of the lattice, which is even overcompensating the effect of thermal expansion in this temperature regime. A secondary effect of dehydration

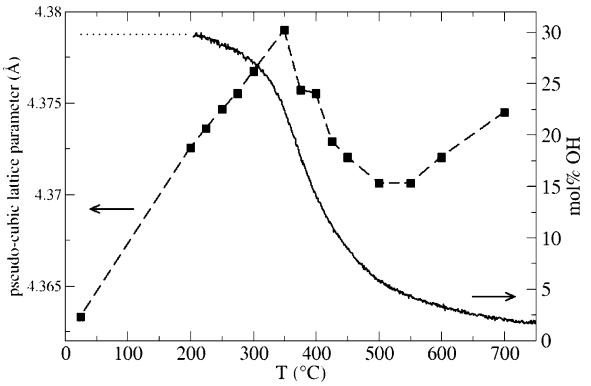

Figure 7. Relation between unit cell (squares and dashed line) and hydration degree in BCI30 (solid line) as a function of temperature in wet N_2 atmosphere. The dotted line represents the extrapolated hydration at low temperatures.

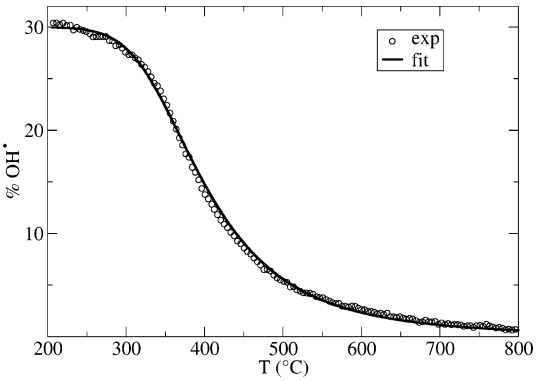

Figure 8. Protonic defect concentration in BCI30 as a function of temperature in wet N_2 atmosphere along with best fit.

Table 2. Thermodynamic Parameters for the Hydration Reaction (eq 1) in Different Proton-Conducting Perovskites

	$\Delta H°$ (kJ/mol)	$\Delta S°$ (J/mol)
$BaCe_{0.7}In_{0.3}O_{3-\delta}$	−81	−105
$BaCe_{0.9}Y_{0.1}O_{3-\delta}$	−163	−168
$BaCe_{0.85}Y_{0.15}O_{3-\delta}$	−176	−178
$BaZr_{0.9}Y_{0.1}O_{3-\delta}$	−79.5	−89
$BaZr_{0.8}Y_{0.2}O_{3-\delta}$	−93	−103
$BaZr_{0.9}In_{0.1}O_{3-\delta}$	−90	−64
$BaZr_{0.9}Gd_{0.1}O_{3-\delta}$	−66	−86

is also the slight decrease of the orthorhombic distortion, as indicated by the differences between $a/4$, $b/\sqrt{2}$, and $c/\sqrt{2}$.

The TGA curves in wet atmosphere have been fitted using a relation given in ref 11 in order to obtain the reaction enthalpy and entropy related to the creation of a protonic defect. For instance, the water incorporation reaction of BCI30, reported in Figure 8, shows a standard enthalpy change of −81 kJ/mol and a standard entropy change of −105 J/mol·K. In Table 2 the standard enthalpy and entropy variations associated with reaction 1 are reported for different 10%-doped proton-conducting perovskites.[1,12,13] These quantities reflect two key features of proton incorporation in the solid state. The enthalpy variation is related to the ability of the oxide to be protonated, i.e., to the oxide basicity. The entropy variation reflects the disorder degree of the protons in the lattice with respect to the water vapor phase. By modeling the TGA data for various perovskites with different dopants it is found that the hydration enthalpy and entropy are somewhat related and that enthalpy and entropy variations

Table 3. Effective Ionic Radius in Octahedral Coordination,[21] Mulliken Electronegativity, and Pearson Absolute Hardness[42] for the Ions under Investigation

	ionic radius (Å)	electronegativity, χ (eV)	hardness, η (eV)
Y^{3+}	0.90	41.2	20.6
Zr^{4+}	0.72	57.9	23.6
In^{3+}	0.80	41	13
Ba^{2+}		22.7	12.7
Ce^{4+}	0.87	51	14.1
Gd^{3+}	0.93	32.3	11.7

for barium cerates are generally much more negative than in zirconates, meaning that basicity and proton ordering are higher in cerates.[1] Recently, Norby et al. proposed a correlation between thermochemical parameters and Allred−Rochow electronegativity of A and B cations.[39] However, this model overlooks the effect of the dopant: rather, we suggest that the nature of the dopant ion is extremely important in determining the entropy and enthalpy of hydration, as discussed below.

Assuming that the contribution of the unprotonated oxide to the entropy variation is the same in the different perovskites, the entropy of protonic defects in the solid state can be reduced either by decreasing the rotational degrees of freedom, as observed by molecular dynamics simulations of protons in $BaCeO_3$,[40] or by reducing the number of degenerate configurations in which the proton can reside. It is clear that the local environment of the dopant, its local symmetry, and the onset of proton−dopant interaction are all key factors that determine the entropy of the hydration reaction. For these reasons we propose that the thermodynamical parameters are strongly dependent on the local environment of the dopant as seen by X-ray absorption spectroscopy. In BCY the dopant fits into the B site without a detectable long-range structural perturbation and the atoms surrounding the dopant site are not significantly displaced from their lattice sites; however, the YO_6 octahedra are distorted, showing the presence of two Y−O bonds with a 0.1 Å difference and the protonic defects preferentially reside in the vicinity of Y^{3+}. In the case of In^{3+}, the dopant significantly displaces the surrounding atoms from their lattice sites, creating some kind of cubic structure hosted in the global orthorhombic matrix. The InO_6 octahedra are very regular, and the protonic defects do not show any preference for residing near the doped B sites. The changes of the host barium cerate lattice caused by the In^{3+} insertion are therefore opposite to those produced by Y^{3+}. It is not surprising then that the thermodynamical parameters reflect this difference, pointing to a disorder of the protonic defects and consequently to a less negative entropy change for the hydration reaction in BCI.

The above experimental evidence concerning the dopant solubility and the interaction of the dopant with the host perovskite lattice cannot be rationalized with the sole reference to ionic radii. In fact, the absolute value of ionic radius mismatch of In^{3+} and Gd^{3+} with Ce^{4+} in octahedral coordination is more than twice that in the case of Y^{3+} doping, so one could expect, taking into account only ionic hindrance, that insertion of the latter into the barium cerate lattice is easier. The definitions of Mulliken electronegativity χ and Pearson total hardness η are as follows[41]

$$\chi = (I + \mathrm{EA})/2 \quad (3)$$

$$\eta = (I - \mathrm{EA})/2 \quad (4)$$

where I is the ionization potential and EA the electron affinity of the chemical species (atom or ion). For a given M^{n+} ion, η is the difference between the nth and $(n + 1)$th ionization potentials and χ is their mean value. A given M^{n+} ion is then classified as "soft" if a small amount of energy is sufficient to modify its electronic configuration, i.e., the ion is easily polarized. The hardness values[42] and ionic radii for the ions discussed in this study are reported in Table 3. We can argue that In^{3+}, being much softer than Y^{3+}, can be more effectively inserted in barium cerate and zirconate host lattices, its low hardness allowing for the resulting strain release, and therefore for structure stabilization. On the contrary, Y^{3+} adapts poorly to insertion in both cerates and zirconates host lattices because of its very high hardness. Other cases of doped oxides confirm this analysis: for fluorite-like ZrO_2:CeO_2 mixed oxides it has been established by EXAFS that the ZrO_8 environment is severely distorted, in contrast with regular CeO_8 cubes.[43,44] A dopant like Gd^{3+}, which is quite soft, leaves the first shell local symmetry unchanged in doped ceria,[45] while the very hard cation Y^{3+} adopts a YO_8 distorted environment with various Y−O bond lengths as in the Y_2O_3 structure.[46]

Preliminary impedance spectroscopy results for BCI with various doping levels yield total conductivities of the order of 0.001 S cm^{-1} at 400 °C, which is quite promising for further development of electrolytes for medium-temperature application. As an example, in Figure 9 the conductivity of

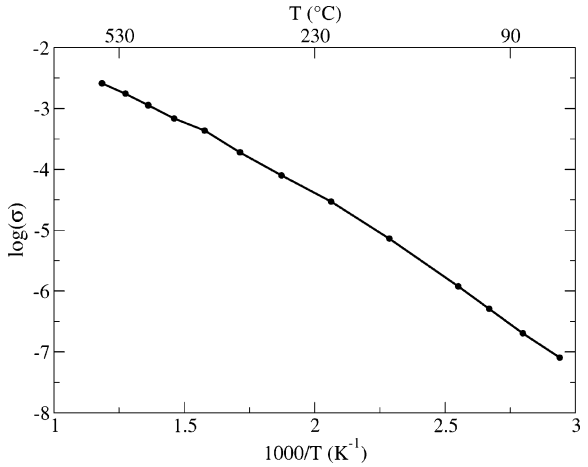

Figure 9. Total conductivity of BCI15 in wet N_2 atmosphere.

(39) Norby, T.; Widerøe, M.; Glöckner, R.; Larring, Y. *Dalton Trans.* **2004**, 3012−3018.
(40) Münch, W.; Kreuer, K.-D.; Seifert, G.; Maier, J. *Solid State Ionics* **2000**, *136*−*137*, 183.
(41) Pearson, R. G. *Inorg. Chem.* **1988**, *27*, 734.
(42) *CRC Handbook of Chemistry and Physics*; CRC Press: Boca Raton, FL, 2005.
(43) Vlaic, G.; Di Monte, R.; Fornasiero, P.; Fonda, E.; Kaspar, J.; Graziani, M. *J. Catal.* **1999**, *182*, 378.
(44) Nagai, Y.; Yamamoto, T.; Tanaka, T.; Yoshida, S.; Nonaka, T.; Okamoto, T.; Suda, A.; Sugiura, M. *Catal. Today* **2002**, *74*, 225.
(45) Inaba, H.; Sagawa, R.; Hayashi, H.; Kawamura, K. *Solid State Ionics* **1999**, *122*, 95.
(46) Wang, Y.; Kageyama, H.; Mori, T.; Yoshikawa, H.; Drennan, J. *Solid State Ionics* **2006**, *177*, 1681.

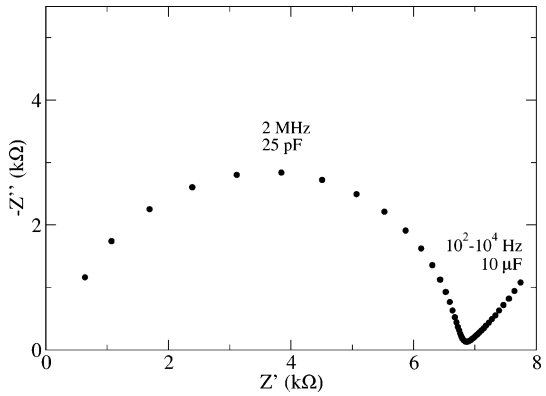

Figure 10. Impedance spectrum of BCI15 in wet N_2 atmosphere at 410 °C. The capacitances for the two elements are reported as calculated from impedance data.

BCI15 is plotted as a function of temperature in the range 50−550 °C. For every sample the activation energy is about 0.56 eV. This value falls into the range of BCY (0.48−0.63 eV)[47] and does not show any change on increasing the dopant concentration. As can be seen in Figure 10, where an IS spectrum for BCI15 is plotted along with capacitance and frequency values, sintering is effective in reducing the grain boundary resistance as no separated grain boundary arc is present between the bulk and the electrode arcs. The latter is not fully recorded because of the limited low-frequency range.

On the basis of our previous findings and the results reported in the present paper, we eventually argue that very high doping levels are also worth investigation and that In^{3+} could be a suitable substitute for doping perovskites in a wide compositional range. Conductivity measurements in the medium-temperature range seem to provide reliable perspectives for electrochemistry applications.

4. Conclusions

The change of the lattice volume in In-doped barium cerate, a proton-conducting perovskite, was studied using XRD. The variation of pseudo-cubic lattice parameter is linear with respect to the dopant concentration, and dopant insertion is effective and easy in the whole compositional range. This also results in high proton concentrations, which may balance the lower proton mobility compared to Y:Ba-CeO_3 for high In-doping levels, yielding promising conductivity values at moderate temperatures. This doping behavior is also suggested to be the consequence of the lower Pearson absolute hardness of In^{3+} compared to Y^{3+}. The proton uptake in In-doped barium cerate was found to be very high, up to the theoretical maximum value for almost every composition. The experimentally determined thermodynamical parameters of the formation (hydration) reaction seem to be critically defined by the local environment of the dopant rather than by the host matrix as they are totally different from values reported for other doped barium cerates. With X-ray absorption spectroscopy (XAS) the local environment of In^{3+} was investigated with the following results. (1) InO_6 octahedra are very regular in every sample. (2) The eight In−Ba distances are all equal in every sample. This is opposed to Ce−Ba distances in orthorhombic barium cerates, which are spread around two values, meaning that the In^{3+} local environment is more symmetrical than the Ce^{4+} one. (3) Debye−Waller factors do not show any large and systematic variation on changing the proton content of the oxide. Following our previous results, this means that protonic defects do not preferentially reside in the vicinity of the dopant.

The results of this paper demonstrate that ionic radius matching is only one and probably, as is confirmed by the behavior of other perovskites, not the most important criterion for tailoring a good proton-conducting ceramic material. As pointed out in ref 1, chemical matching is even more important than the structural one. The high dopant solubility is a further parameter to be taken into account for development of perovskite oxides for electrochemical applications.

Acknowledgment. We thank Gabriele Götz (MPI-FKF) for the XRD measurements and Rotraut Merkle (MPI-FKF) for reading the proofs. We acknowledge the European Synchrotron Radiation Facility for provision of synchrotron radiation facilities and Chiara Maurizio and Francesco d'Acapito for assistance in using beamline GILDA BM8. Partial financial support from Ministero dell'Università e della Ricerca (PRIN 2006 Ceramici protonici per celle a combustibile and FISR Progetto celle a combustibile) and from Università di Palermo (ex 60%) is acknowledged.

CM701902P

(47) Kreuer, K.-D.; Dippel, T.; Baikov, Y. M.; Maier, J. *Solid State Ionics* **1996**, *86−88*, 613.